

## Fabrication and nano structural study on $\text{La}_2\text{O}_3\text{-Co}_3\text{O}_4\text{-ZrO}_2$ composite

### ABSTRACT

**N. Aghaeenejad**<sup>1</sup>  
**A. Bahari**<sup>2</sup>  
**M. Riazian**<sup>3,\*</sup>  
**M. Ghanbari**<sup>4</sup>

<sup>1</sup>Department of Physics,  
Mazandaran Science and  
Research Branch, Islamic Azad  
University, Mazandaran, Iran.

<sup>2</sup>Department of Physics,  
University of Mazandaran,  
Babolsar, Iran.

<sup>3</sup>Department of Engineering,  
Tonekabon branch, Islamic Azad  
University, Tonekabon, Iran.

<sup>4</sup>Department of Physic, Islamic  
Azad University, Central  
Tehran Branch, Iran.

We report on the synthesis, morphology, chemically and structurally of  $\text{La}_2\text{O}_3\text{-Co}_3\text{O}_4\text{-ZrO}_2$  nanostructure. The  $\text{La}_2\text{O}_3\text{-Co}_3\text{O}_4\text{-ZrO}_2$  nanostructure was synthesized by a method based on the co-precipitation. Composite powders have been characterized by XRD (X-ray diffraction), SEM (scanning electron microscopy) and BET (Brunauer-Emmett-Teller). X-ray diffraction showed the formation of nano crystalline,  $\text{La}_2\text{Zr}_2\text{O}_7$ ,  $\text{ZrO}_2$ ,  $\text{La}(\text{OH})_3$  and  $\text{Co}_3\text{O}_4$  phases. Scanning electron microscopy revealed that nanostructure formed by increasing the calcinations temperatures. With BET and BJH (Barrett, Joyner and Halenda) method the pore size distribution was determined. The effects of chemical compositions and calcinations temperature on the surface topography and the crystallization of phases were studied. The lattice strain of nanocrystallite during thermal treatment was calculated.

**Keywords:** *Fabrication; Nanostructure;  $\text{La}_2\text{O}_3\text{-Co}_3\text{O}_4\text{-ZrO}_2$ ; Composite; Co-precipitation.*

Received 17 August 2013

Accepted 02 December 2013

### INTRODUCTION

Mixed metal oxides comprise the vast majority of catalysts used in modern chemical industry. Among the mixed metal oxides, Cobalt oxide ( $\text{Co}_3\text{O}_4$ ) powder has a wide range of applications in various fields of industry including anode materials for rechargeable Li-ion battery, catalyst, gas sensor and magnetic materials [1–4].

The properties of  $\text{Co}_3\text{O}_4$  in above applications are highly related to the particle size. It has been indicated that nanocrystalline  $\text{Co}_3\text{O}_4$  is especially good for the property promotion [5]. Much effort has been made to prepare  $\text{Co}_3\text{O}_4$  nanoparticles, including pulsed laser deposition [6], sol–gel route [7], reduction–oxidation route [8], gel hydrothermal oxidation [5], homogeneous precipitation [9], staged oxidation process [10] and cobalt salt decomposition [11,12], but through all of the above methods, nanocrystalline  $\text{Co}_3\text{O}_4$  is more difficult and inconvenient to obtain.

\* Corresponding author:

M. Riazian  
Department of Engineering,  
Tonekabon branch, Islamic Azad  
University, Tonekabon, Iran.  
Tel +98 9120116905  
Fax +98 1924274415  
Email [m.riazian@toniau.ac.ir](mailto:m.riazian@toniau.ac.ir)

In general, the potential commercial cobalt catalysts are typically composed of four components: Co metal, a small amount of a second metal, oxide promoters (alkali, rare earth, and/or transition metal oxide such as  $ZrO_2$ ) and supports (Silica, Alumina or Titania) [13,14]. Modification of Zirconia by a second metal, therefore, could improve its properties as a catalyst support. Previous studies have shown that the catalytic activities of Co catalysts in CO hydrogenation were improved by the use of  $ZrO_2$  mixed oxides such as  $Al_2O_3-ZrO_2$  [15] and  $SiO_2-ZrO_2$  [16]. Lanthanum, one of interesting rare earth promoters for cobalt catalyst, was reported to be beneficial for CO hydrogenation to produce long chain hydrocarbons and it showed a significant enhancement of catalytic activity owing to increase of active site dispersion [17,18]. Solid-state reaction of La and Co oxides at high temperature results in the formation of large particle size and limited degree of chemical homogeneity. Fine and homogeneous particles with high specific surface area are formed during a chemical solution process, such as citrate method, using different starting precursors, usually nitrate and an organic additive such as citric acid [19].

In this study,  $La_2O_3-Co_3O_4-ZrO_2$  nanocomposite was prepared by Co-precipitation method. The morphologies and the crystalline structures of the  $La_2O_3-Co_3O_4-ZrO_2$  are characterized using FE-SEM, AFM, TEM, XRD, and BET. We have suggested the optimum experimental conditions for the various composite particle syntheses.

## EXPERIMENTAL

The composition of the starting solution and the experimental conditions used for ternary powders are listed in Table 1. The  $La_2O_3-Co_3O_4-ZrO_2$  was prepared separately by mixing precursors:  $(Co(NO_3)_2 \cdot 6H_2O)$  (Merck  $\geq 99\%$ ), Water,  $HNO_3$ ),  $(ZrOCl_2)$  (Merck  $\geq 99\%$ ), water, acetic acid (Fluka, 60%), ethanol (Merck  $\geq 99\%$ ),  $(La(NO_3)_3)$  (Fulka  $\geq 99\%$ ), water,  $HNO_3$ ) at room temperature and then these solutions were combined with together and after 72 h, gelation was formed. This gel also was dried for 12 h at  $80^\circ C$  and then was washed thoroughly with distilled water to eliminate

the chloride ions. This powder calcined at 600 and  $800^\circ C$ .

**Table 1.** Composition of starting solutions and experimental conditions for ternary powders preparation

Co-precipitation method	Precursor and Molar ratio(MR)	Stirring Time(h)	pH
	$Co(NO_3)_2 \cdot 6H_2O / ZrOCl_2 / La(NO_3)_3 = 1$	72	8

## Characterization of the $La_2O_3-Co_3O_4-ZrO_2$

XRD patterns measured on a (GBC-MMA 007 (2000)) X-ray diffractometer. The diffractograms recorded with  $(K\alpha(Cu), 1.54056\text{\AA}, 0.02^\circ)$  step size in which the speed  $10^\circ/\text{min}$  radiation over a  $2\theta$  range of  $10^\circ-70^\circ$ . The  $N_2$  adsorption-desorption isotherms are obtained by on a Sorptometer Kelvin 1042 at  $77^\circ K$ , from which the surface area ( $S_{BET}$ ), the pore volume ( $V_p$ ) and the pore diameter ( $d_p$ ) are calculated by BET and BJH methods, respectively.

## RESULTS AND DISCUSSION

Crystallographic phases of the composite were investigated by XRD method. Figure 1 and assignments of the XRD peaks are summarized in Table 2, respectively. Due to different hydrothermal treatment crystalline phases are formed. Figure 1 shows the XRD patterns of powder obtained from gels after drying and calcination at  $600^\circ C$  and  $800^\circ C$  with  $10 \frac{^\circ}{\text{min}}$  gradient and stayed in 2 hours, after then, they cooled in similar temperature gradient. Figure 1 shows the amorphous structure for as-prepared sample due to the short range ordering of the network [20]. Samples obtained from  $600^\circ C$  and  $800^\circ C$  have a high degree of the crystallinity. The grain size values were calculated from Scherrer equation:

$$d = \frac{0.9 \lambda}{2B \cos \theta'} \quad (1)$$

Where  $\lambda = 0.154$  nm, and  $\theta$  is the reflection angle.

As shown in Figures 1, there is only  $Co_3O_4$  phase (peak at  $2\theta = 37.1^\circ$ ). The size of grains

increases with increasing the calcination temperature corresponds to Table 2.

Lattice strains of nanocrystallites are determined from the dependence of FWHM of diffraction lines observed in  $2\theta$  range of  $10-80^\circ$  on  $\sin\theta$ , according to the Williamson-Hall's equation [21]:

$$\beta \cos\theta = \frac{k\lambda}{L} + 4\sin\theta, \quad (2)$$

Where  $\beta$  was FWHM observed, shape factor  $k$  was assumed to be 0.9 similar to Scherrer equation's.  $\lambda$  (wavelength of  $K_\alpha$  (Cu)). The plots of  $\beta \cos\theta$  against  $4\sin\theta$  for different samples were

approximated to be linear. Lattice strain was determined from the slop of this linear relation. Because of lowly-crystallized powder samples, the linearity between  $\beta \cos\theta$  and  $4\sin\theta$  is not very evident [22]. The plots of  $\beta \cos\theta$  against  $4\sin\theta$  for different diffraction lines are illustrated in Figure 2. For low calcined temperatures, the experimental points for the diffraction lines measured scattered, because the peaks are weak and broad so that their FWHMs were difficult to be measured. As can be seen in Figure 2, the lattice strain increases from 0.2597 (of  $600^\circ\text{C}$ ) to 0.4179 (of  $800^\circ\text{C}$ ) calcinations temperature.

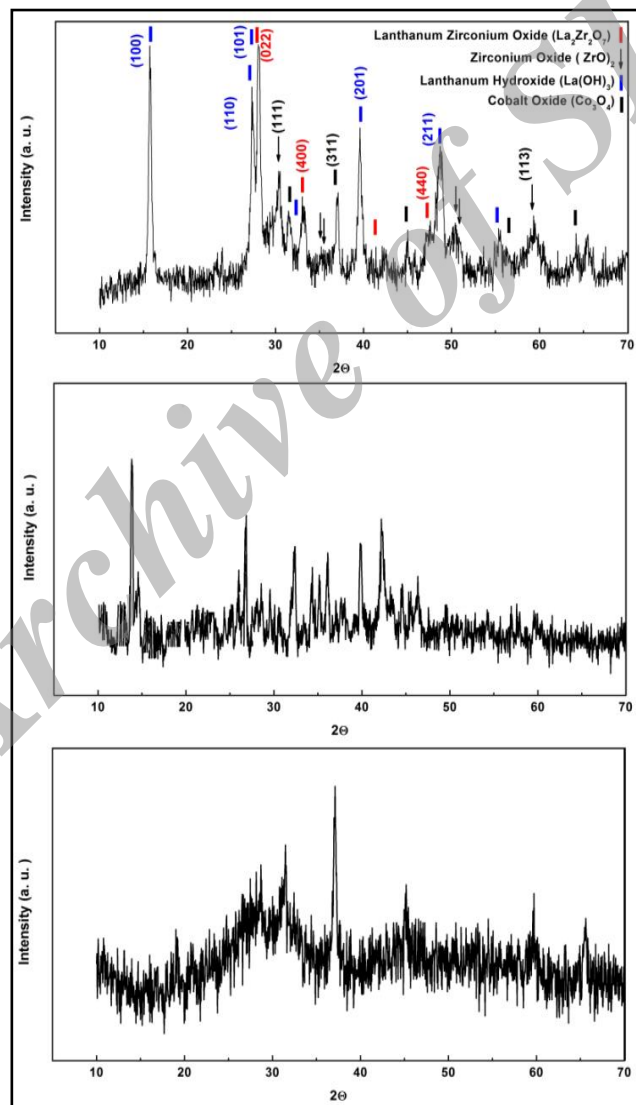
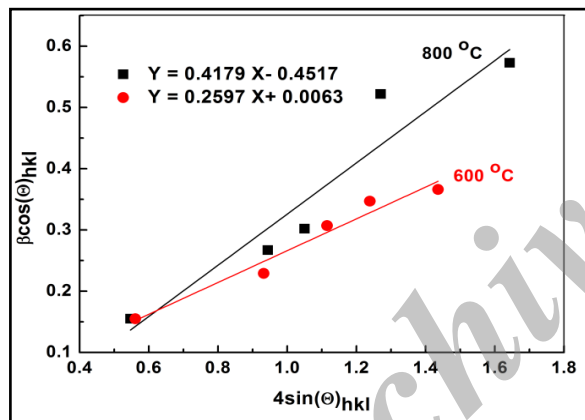


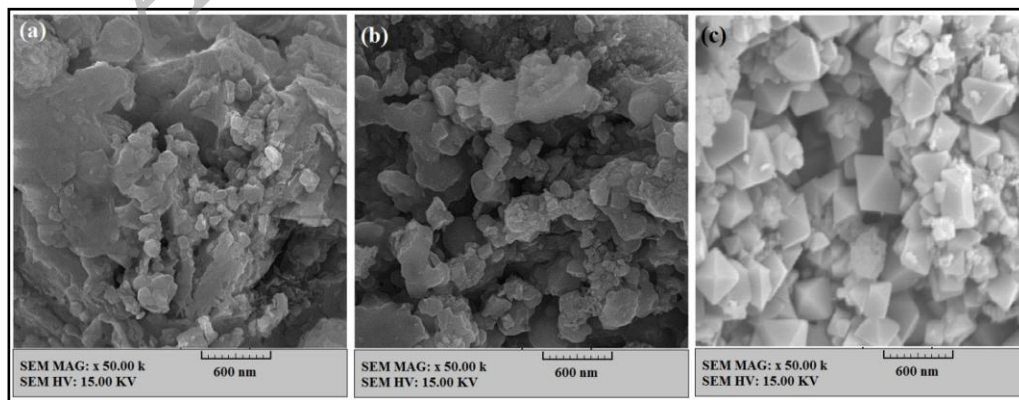
Fig. 1. XRD patterns of  $\text{La}_2\text{O}_3\text{-Co}_3\text{O}_4\text{-ZrO}_2$  (a) without calcination temperature (as-prepared), (b) calcined at  $600^\circ\text{C}$  and (c) calcined at  $800^\circ\text{C}$ .

**Table 2.** The  $2\theta$  angle, d-space, Miller indexes, grain size and lattice strain of  $\text{La}_2\text{O}_3\text{-Co}_3\text{O}_4\text{-ZrO}_2$ .

Crystalline Phase	As-prepared			Calcined at 600 °C			Calcined at 800 °C		
	$2\theta$	d-space(Å)	size(nm)	$2\theta$	d-space(Å)	size(nm)	$2\theta$	d-space(Å)	size(nm)
<b><math>\text{La}_2\text{Zr}_2\text{O}_7</math></b> Cubic a=10.823 Å		-----		28.08	3.15	4	28.15	3.17	4
<b><math>\text{ZrO}_2</math></b> Cubic a=5.1030 Å		-----		30.61	2.91	3	30.471	2.93	4
<b><math>\text{La(OH)}_3</math></b> Hexagonal a=6.5286 Å c=3.859 Å		-----		16.00	5.50	6	15.81	5.59	10
<b><math>\text{Co}_3\text{O}_4</math></b> Cubic a=8.0840 Å	37.10	2.41	3	36.95	2.41	5	37.06	2.42	8

**Fig. 2.** The relation between  $\beta\cos\theta$  and  $4\sin\theta$  (Williamson-Hall plots) with different calcination temperatures.

SEM images of  $\text{La}_2\text{O}_3\text{-Co}_3\text{O}_4\text{-ZrO}_2$  nanopowders are shown as Figure 3(a-c). In Figure 3(a), as-prepared powder sample has irregular surface. As shown in Figure 3, SEM images of powders with different calcination temperatures are presented. Nanoparticles have more congestion and density with increasing the calcination temperature also, with increasing the calcination temperature, nanoparticles become tetragonal-shape. It is obvious that larger particle size is achieved by increasing the calcinations process and this is in good consistence with the Scherrer's equation in the XRD evaluation.

**Fig. 3.** SEM images of powder samples for MR=0.5 (a) as-prepared, (b) 300 °C, (c) 600 °C, (d) 800 °C.

Additional characteristic parameters of the sample with 800 °C calcination temperature (such as BET surface area, mean pore diameters) are calculated by BET and BJH methods. According to the BET method data particles have a specific surface area of 12.039 m<sup>2</sup>/g and the mean pore diameter of 24.262 nm and total pore volume 0.07302 cm<sup>3</sup>/g. We can notice from BJH method (Figure 4(a-c)) that the pore size distribution (peak) is 5.29 nm.

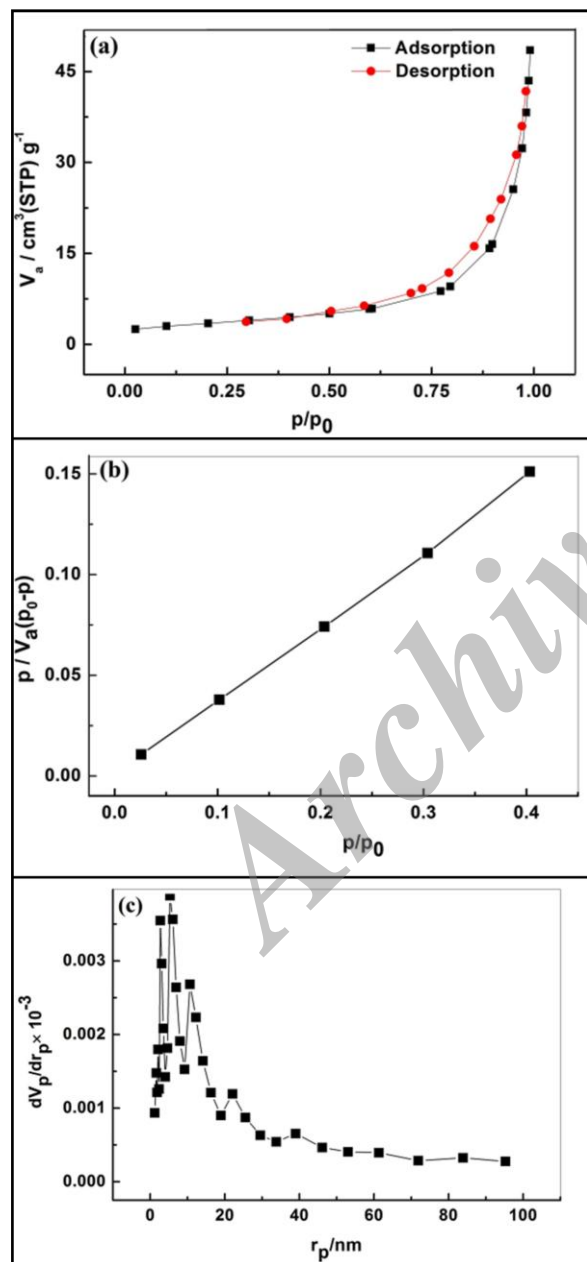


Fig.4. (a) Isotherm adsorption-desorption plot, (b) BET plot, (c) BJH plot.

## CONCLUSIONS

Experimental results indicate that the homogeneous synthesis of La<sub>2</sub>O<sub>3</sub>-Co<sub>3</sub>O<sub>4</sub>-ZrO<sub>2</sub> composite via co-precipitation route is a promising technique for preparing material with uniform nanoparticles. In this study, nanocrystalline La<sub>2</sub>O<sub>3</sub>-Co<sub>3</sub>O<sub>4</sub>-ZrO<sub>2</sub> particles have been successfully synthesized by chemical method and heat treatment process. The effect of La<sub>2</sub>O<sub>3</sub>-Co<sub>3</sub>O<sub>4</sub>-ZrO<sub>2</sub> composite on the structural properties of powders by co-precipitation technique has been examined. The XRD spectra show La<sub>2</sub>Zr<sub>2</sub>O<sub>7</sub>, ZrO<sub>2</sub>, La(OH)<sub>3</sub> and Co<sub>3</sub>O<sub>4</sub> phases and grains size. The size of grains increase with increasing the calcination temperature corresponds to Table 2. Scanning electron microscopy measurements show nanostructure and morphology of powders. With increasing the calcination temperature, nanoparticles become tetragonal-shape and larger particle size is achieved by increasing the calcination temperature. It has been shown that with increasing the calcination temperature lattice strain increases from 0.2597 (of 600 °C) to 0.4179 (of 800 °C) calcination temperatures.

## REFERENCES

- [1] Koinuma M., T. Hirae, Matsumoto Y., (1998), Electrochemical preparation of cobalt oxide using an autoclave electrolytic. *Cell. J. Mater. Res.* 13: 837-839.
- [2] Jansson J., Palmqvist A. E. C., Fridell E., (2002), On the Catalytic Activity of Co<sub>3</sub>O<sub>4</sub> in Low-Temperature CO Oxidation. *J. Catal.* 211: 387-397.
- [3] Choi S. D., Min B. K., (2001), Co<sub>3</sub>O<sub>4</sub>-based isobutane sensor operating at low temperatures. *Sens. Actuators. B.* 77: 330-6.
- [4] Makhlof S. A., Magn J., (2002), Magnetic Properties of Co<sub>3</sub>O<sub>4</sub> Nanoparticles, *Magn. Mater.* 246: 184-190.
- [5] Jiang Y., Wu Y., Xie B., Qian Y., (2002), Moderate temperature synthesis of nanocrystalline Co<sub>3</sub>O<sub>4</sub> via gel hydrothermal

- oxidation. *Mater. Chem. Phys.* 74: 234-237.
- [6] Koshizaki N., Narazaki A., Sasaki T., (2001), Size distribution and growth mechanism of  $\text{Co}_3\text{O}_4$  nanoparticles fabricated by pulsed laser deposition. *Scr. Mater.* 44: 1925-1928.
- [7] Svegl F., Orel B., Grabec I., Kaucic V., (2000), Characterization of spinel  $\text{Co}_3\text{O}_4$  and Li-doped  $\text{Co}_3\text{O}_4$  thin film electrocatalysts prepared by the sol-gel route. *Electrochim. Acta* 45: 4359-4371.
- [8] Ni Y., Ge X., Zhang Z., Liu H., (2001), A simple reduction-oxidation route to prepare  $\text{Co}_3\text{O}_4$  nanocrystals. *Mater. Res. Bull.* 36: 2383-3287.
- [9] Zhu X., Liao L., Chui Y., (2001), One-dimensional arrays of  $\text{Co}_3\text{O}_4$  nanoparticles: synthesis, characterization, and optical and electrochemical properties. *Inorg. Chem. Ind.* 34: 1-7.
- [10] Zeng H.C., Lim Y. Y., (2000), Effect of annealing on fluorescence of  $\text{Ce}^{3+}$ -doped silica prepared by sol-gel process. *J. Mater. Res.* 15: 1250-56.
- [11] Furlanetto G., Formaro L., (1995), Precipitation of Spherical  $\text{Co}_3\text{O}_4$  Particles. *J. Collo. Interf. Sci.* 170: 169-175.
- [12] Ardizzone S., Spinolo G., Trasatti S., (1995), The point of zero charge of  $\text{Co}_3\text{O}_4$  prepared by thermal decomposition of basic cobalt carbonate. *Electrochim. Acta* 40: 2683-7.
- [13] Haddad G. J., Chen B., Goodwin J. G. (1996), Characterization of  $\text{La}_2\text{O}_3$ -promoted  $\text{Co}/\text{SiO}_2$  catalysts. *J. Catal.* 160: 43-51.
- [14] Iglesia E., (1997), Design, synthesis, and use of cobalt-based Fischer-Tropsch synthesis catalysts. *Appl. Catal. A.* 61: 59-78.
- [15] Soisuwan S., Panpranot J., Trimm D. L., Prasertdam P., (2006), A study of Alumina-Zirconia mixed Oxides prepared by the modified Pechini as Cobalt catalyst supports in CO hydrogenation. *Appl. Catal. A. Gen.* 303: 268-272.
- [16] Jongsomjit B., Kittiruangrayub .S, Prasertdam P., (2007), Study of cobalt dispersion onto the mixed nano- $\text{SiO}_2$ - $\text{ZrO}_2$  supports and its application as a catalyst phase. *Mater. Chem. Phys.* 105: 14-19.
- [17] Khodakov A. Y., Chu W., Pascal F., (2007), Advance in the development of novel Fischer-Tropsch catalyst for synthesis of long chain hydrocarbon and clean fuel. *Chem. Rev.* 107: 1692-1744.
- [18] Wang T., Ding Y., Lu Y., Zhu H., Lin L., (2008), Influence of lanthanum on the performance of Zr-Co/ activate dcarbon catalysts on Fischer-Tropsch synthesis. *J Natur. Gas Chem.* 17: 153-158.
- [19] Hwang H. J., Moon J., Awano M., Maeda K., (2000), Design of multi-layered electrochemical cell for exhaust gas purification. *J. Am. Ceram. Soc.* 83: 2852-5.
- [20] Hochbaum A. I., Fan R., He R., Yang P., (2005), Controlled Growth of Si Nanowire Arrays for Device Integration. *Nano Lett.* 5: 457-460.
- [21] Carp O., Huisman C. L., Reller A., (2004), Photoinduced reactivity of titanium dioxide. *Prog. Solid State Chem.* 32: 33-177.
- [22] Inagaki M., Nonaka R., Tryba B., Morawski A. W., (2006), Dependence of photocatalytic activity of anatase powders on their crystallinity. *Chemosphere.* 64: 437-445.